Journal of Metals, Materials and Minerals, Vol. 30, No. 1, pp. 29-39, 2020

On the corrosion behaviour of as-cast and heat-treated Mg-RE alloys in 0.9% NaCl solution

Abdelkader HANNA[1], Lyacine RABAHI[2,3], Mohamed Amine SOUALILI[3], Achour DAKHOUCHE[4], Djamel BRADAI[5], and Hiba AZZEDDINE[1,*]

[1] *Department of Physics, Faculty of Sciences, University of Mohamed Boudiaf, M'sila, 28000, Algeria*
[2] *Laboratoire de Physique Théorique, Faculté de Physique, USTHB, BP 32, El Alia, 16111, Bab Ezzouar, Alger, Algeria*
[3] *Research Center in Industrial Technologies CRTI. P.O. Box 64, Cheraga, Algiers, 16014, Algeria*
[4] *Inorganic Materials Laboratory, Department of chemistry, Faculty of Sciences, University of Mohamed Boudiaf, M'sila, 28000, Algeria*
[5] *Faculty of Physics, University of Sciences and Technology HouariBoumedienne, BP 32 El Alia Bab Ezzouar, Algiers, Algeria*

[*]**Corresponding author e-mail:** hiba.azzeddine@univ-msila.dz

Received date:
25 September 2019
Revised date:
22 December 2019
Accepted date:
9 January 2020

Keywords:
Corrosion resistance
Heat treatment
Magnesium alloy
NaCl solution
Rare earth

Abstract

The microstructure and corrosion behaviour of as-cast and heat-treated Mg-1.44Nd and Mg-1.43Ce (wt.%) alloys in 0.9% NaCl (wt.%) solution were investigated using electrochemical tests, X-ray diffraction (XRD) and scanning electron microscopy, combined with energy-dispersive X-ray spectroscopy (SEM-EDS). The as-cast microstructure of both alloys revealed the presence of second phases. Heat treatment at 535°C for 6 h led to a more uniform distribution of the second phases in Mg-1.44Nd alloy and their dissolution along the grains boundaries in the Mg-1.43Ce alloy. As a result, the corrosion resistance was improved in the heat-treated alloys. Accordingly, the corrosion resistance values for the heat-treated alloys were much higher than those of the as-cast alloys, indicating that the heat-treated alloys were less susceptible to the corrosion. Also, the heat-treated Mg-1.43Ce alloy seems to have very good corrosion resistance (26890 Ω cm^2) compared to the Mg-1.44Nd alloy (6156 Ω·cm^2) by preventing pitting corrosion along the grains boundaries. The corrosion product was made up mainly of magnesium hydroxide $Mg(OH)_2$ and magnesium oxide MgO and more uniform corrosion morphology were found in the heat-treated alloys.

1. Introduction

The low density (ρ ~ 1.74 g·cm^{-3}) and high specific strength (123-144 MPa·g·cm^{-3}) of magnesium-based alloys make them excellent candidates for lightweight structural applications such as the automotive and aerospace industries [1,2]. Moreover, Mg-based alloys are receiving increasing attention as potential biodegradable implant materials in biomedical applications, thanks to their biodegradability [3]. However, these alloys generally suffer from poor corrosion resistance in aqueous environments, and their degradation occurs faster than expected in different environments which limited their use in a variety of applications [4-6]. The presence of impurities and the inhomogeneous distribution of second phases are the main causes of galvanic corrosion and thereby of poor corrosion resistance [3]. Therefore, challenging analyses must be conducted to optimise the distribution of second phases to obtain uniform corrosion in Mg-based alloys. Thermo-mechanical processing and/or alloying elements have proven their effectiveness in modifying the microstructure by decreasing grain size as well as changing the distribution of second phases [7-15]. For example, high-pressure torsion (HPT) processing leads to uniform corrosion compared to localised corrosion, as occurs in as-cast pure Mg [9]. However, some contradictory findings have been reported for pure Mg and AZ91 alloys after grain refinement by severe plastic deformation (SPD), where the as-cast samples exhibits a higher corrosion resistance than the deformed ones in 3.5 wt% NaCl solution [16,17]. Theoretically, decreasing the grain size involves increasing the number of grain boundaries and it is known that grain boundaries are more corrosion active than the bulk, which could explain the lower corrosion resistance in the deformed samples. Recently, it has been suggested that the crystallographic orientation of grains may be responsible for the changes in corrosion behaviour in deformed Mg-based alloys [18-20].

It has been reported that rare earth (*RE*) elements have a beneficial effect on the corrosion resistance of Mg-based alloys, mainly owing to the formation of intermetallic compounds with impurities during the melting process [21] or the passivation cathode effect of the second phases [22]. Moreover, the presence of the RE element in the corrosion product film considerably improves the corrosion resistance of the Mg-based alloys [23].

DOI: 10.14456/jmmm.2020.4

The corrosion resistance of forged Mg-6.7Zn-1.3Y-0.6Zr alloy (wt%) was improved by the solution treatment at 300°C for 1 h and 400°C for 2 h, mainly owing to the dissolution of $MgZn_2$ precipitates [24].Contradictory reports indicate that the presence of the second phase considerably increases the corrosion rate of Mg-based alloys [25,26]. The temperature and the duration of annealing treatment conditions lead to different microstructural changes, such as to the composition, size, shape, distribution and volume fraction of the second phases, thereby having a larger influence on the corrosion behaviour of Mg-based alloys [25-28].

The effect of heat treatments on the corrosion resistance of Mg-based alloys is still not fully understood. Accordingly, the aim of the present study is to investigate the effect of heat treatment at 535 °C for 6 h on the microstructure and corrosion behaviour of two as-cast binary Mg-1.44Nd and Mg-1.43Ce (wt%) alloys in a 0.9% NaCl (wt%) solution, using electrochemical tests, XRD, SEM and EDS.

2. Experimental Procedure

The as-cast Mg-1.44Nd (wt%) and Mg-1.43Ce (wt%) alloys were kindly supplied by colleagues from the Institut für Metallkunde und Metallphysik (IMM), Aachen, Germany. The alloys were prepared by induction melting and casting in a protective atmosphere of Ar/CO_2 gas, followed by heat treatment for 20 h at 420°C. After that, both alloys underwent a partial solution annealing in a controlled atmosphere at 535°C for 6 h. The selected temperature (535°C) and duration (6 h) were chosen in order to avoid excessive sublimation of the Mg and to insure a correct Nd and Ce solute diffusion in Mg matrix.

Scanning electron microscopy (SEM, FEG-SEM ZEISS Gemini) was used to visualise the microstructures in as-cast and heat-treated alloys and after the immersion test. Energy-dispersive spectrometry (EDS) system in backscattering (BSE) mode operated at 15 kV was performed to determine the composition of the second particles and the corrosion product.

X-ray diffraction (XRD) patterns were recorded using an X'PERT PRO MPD diffractometer operating at 40 kV and 40 mA, using Cu-Kα radiation. The data were collected over a range of 2θ = 20-90° with a step size of 0.026° and a scan speed of 0.18°/sec.

The electrochemical tests were carried out using AUTOLAB PGSTAT302N, with a three-electrode system, platinum plate as a counter electrode, a calomel electrode (SCE) (0.24 vs. SHE) as the reference electrode and the sample as a working electrode. The samples were embedded in an epoxy resin to isolate a 0.5 cm2 area and then immersed at room temperature in a 0.9% NaCl (wt%) solution. The open-circuit potential (OCP) was measured for at least 2 h for all samples. The polarisation curves were measured in the range of -2.6 to 0 V vs. SCE with a scan rate of 2 $mV \cdot s^{-1}$.

Impedance measurements were performed after a steady state of 2 h using a sinusoidal potential signal with an amplitude of 10mV, in the frequency range from 10^5Hz to 10^{-2}Hz. The curves were fitted using Zview software.

3. Results and discussion

Figure 1 shows the microstructures of as-cast and heat-treated Mg-1.44Nd and Mg-1.43Ce alloys, respectively. It was reported earlier that both alloys exhibit an elongated granular microstructure with a large grain size of approximately 400 μm [29]. As can be seen from Figure 1, the microstructures of as-cast and heat-treated for both alloys show the presence of different second phases. Table 1 summarises the EDS analysis (in wt%) at several positions (points 1–8) in the microstructures of thealloys. The volume fractions of the second phase are also shown in Figure 1. The solubility of Ce (0.27% at 590°C) and Nd (3.6% at 552°C) in the Mg matrix is relatively low [30]. Therefore, the formation of these particles is unavoidable during the melting and cooling of these alloys.

The heat treatment at 535°C for 6 h failed to dissolve the second phases and obtain a homogeneous microstructure. However, some differences could be noticed between the as-cast and heat-treated conditions for both alloys. The microstructure of as-cast Mg-1.44Ndalloy presents three different second phases: $Mg_{41}Nd_5$ (point 1), $Mg_{12}Nd$ (point 2) and particles (point 3), with a small amount of Nd element ~17.6%. The apparent diameter of these particles is in the range of 3-8 μm.

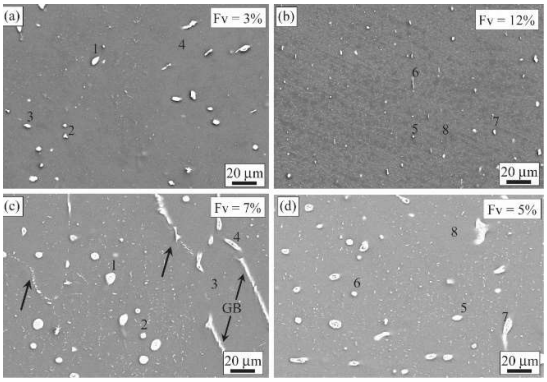

Figure 1. SEM micrographs showing the microstructure of (a) as-cast Mg-1.44Nd, (b) heat-treated Mg-1.44Nd, (c) as-cast Mg-1.43Ce, and (d) heat-treated Mg-1.43Ce alloy.

These second phases are still present even after the heat treatment, as shown in Figure 1(b) and Table 1 (points 5-7), but are very small in size (in the range of 2-4 μm).

Table 1. EDS analysis in weight percentage at several positions in the microstructures (shown in Figure 1) of the as-cast and the heat-treated Mg-1.44Nd and Mg-1.43Ce alloys, respectively.

Mg-1.44Nd Element (wt%)	**1**	**2**	**3**	**4**	**5**	**6**	**7**	**8**
Mg	59.36	39.11	82.38	98.95	51.34	93	78.54	96.82
Nd	40.64	60.89	17.62	1.05	48.66	7	21.46	3.18
Mg-1.43Ce Element (wt%)	**1**	**2**	**3**	**4**	**5**	**6**	**7**	**8**
Mg	70.63	84.599	99.54	85.62	70.68	81.34	70.86	99.61
Ce	29.37	15.41	0.46	14.38	29.32	18.66	29.14	0.39

The heat treatment of Mg-1.44Nd alloy seemed to cause the formation of new second phases, with white spots distributed almost uniformly in the microstructure. In fact, the volume fraction of second phases increases from 3 to 12% after heat treatment. Unfortunately, the identification of their chemical composition was not possible by EDS analysis because of their very small size. The concentration of Nd element in the matrix (point 4, 1.05%) increases after the heat treatment (point 8, 3.18%), which could be attributed to the development of these tiny particles.

The heat treatment at 535°C for 6 h affects the microstructures of as-cast Mg-1.43Ce alloy differently. Besides the presence of several circular particles identified as $Mg_{12}Ce$ (point 1) and particles with 15% of Ce (point 2), in sizes ranging from 5 to 10 μm, and very small particles distributed within the grains, the second phases are also found in the grains boundaries, as shown by the arrow in Figure 1(c). It is interesting to note that the heat treatment of as-cast Mg-1.43Ce causes an apparent dissolution of the second phase along the grains boundaries. Nevertheless, the particles present within the grains seem to be stable and not affected by the heat treatment, as indicated by their slight decrease from 7 to 5%. On the other hand, the second $Mg_{41}Nd_5$ phase was not identified by XRD patterns, perhaps because of their small amount in the microstructure. The presence of stable particles in the Mg-1.43Ce alloy is attributed to the low solubility of Ce in the Mg matrix (0.27%) [30]. In contrast, the Nd element seems to be more distributed into the Mg matrix since its solubility in the Mg matrix (3.6%) is much higher than that of Ce [30].

The XRD patterns of as-cast and heat-treated Mg-1.44Nd and Mg-1.43Ce alloys are shown in Figure 2. All peaks in as-cast and heat-treatedMg-1.44Nd alloy belong to the Mg matrix, except the one located at 2 θ = 45°, identified as $Mg_{12}Nd$ second phase. The XRD patterns of as-cast and heat-treated Mg-1.43Ce alloy revealed the presence of $Mg_{12}Ce$ and $Mg_{17}Ce_2$phases. It should be noted that the second $Mg_{17}Ce_2$ phase particles were not identified by EDS analysis may be due to their small size and/or volume fraction.

The XRD patterns show clearly that heat treatment has a great influence on the crystallographic orientation of the grains in both alloys. For example, the intensity of (112) peak at 2θ = 68.87° decreases drastically after heat treatment of the Mg-1.44Nd alloy and the (002) peak at 2θ = 34.32° is the highest, indicating the formation of basal texture after heating. Similar observations can be made for peaks (110) at 2θ = 32.28° and (101) at 2θ = 34.45° in the case of the Mg-1.43Ce alloy (Figure 2(b)).

Figures 3(a) and 3(b) present the potentiodynamic polarisation curves of as-cast and heat-treated Mg-1.44Nd and Mg-1.43Ce alloys in a 0.9% NaCl solution, respectively. The fitted corrosion potential E_{corr}, the corrosion current density I_{corr}, β_a anodic, β_c cathodic Tafel slopes and the polarisation resistance R_p listed in Table 2 were determined by extrapolating the linear Tafel segments of the anodic and cathodic branches.

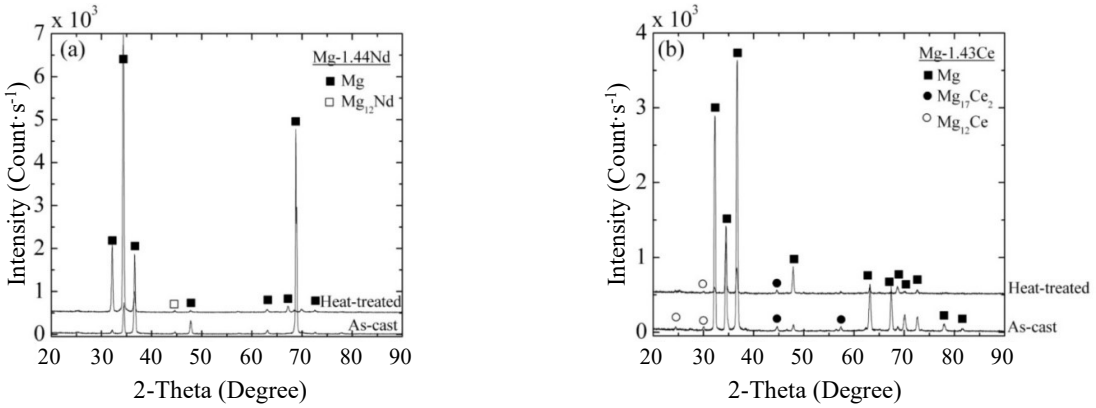

Figure 2. XRD patterns of as-cast and heat-treated: (a) Mg-1.44Nd and (b) Mg-1.43Ce alloys.

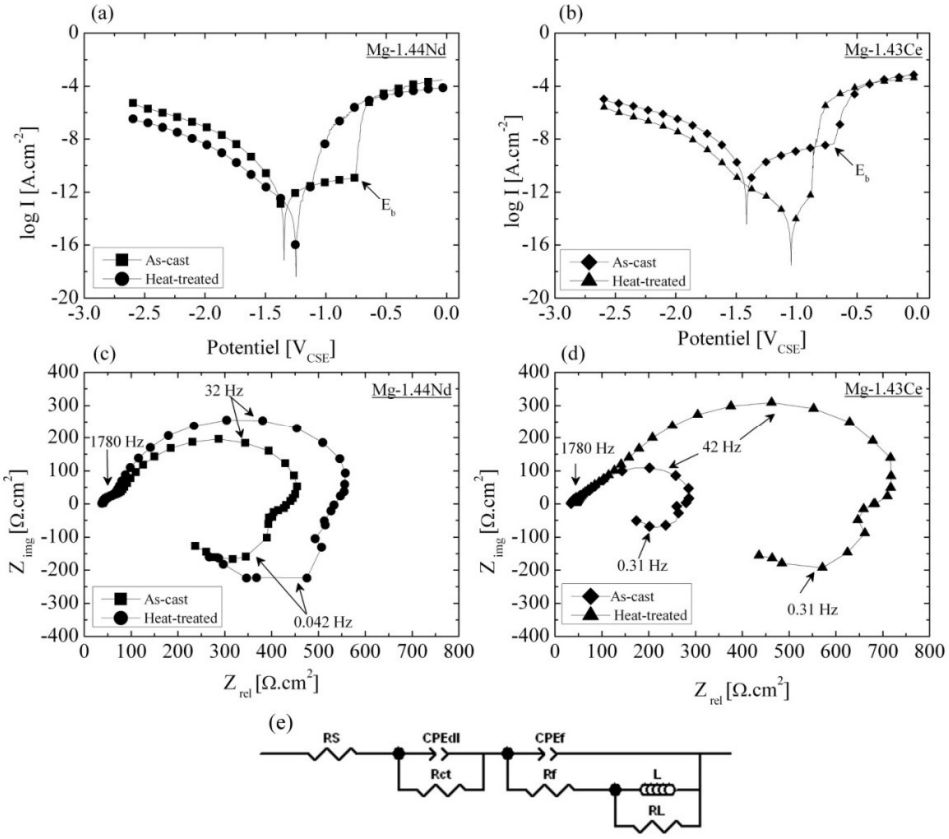

Figure 3. (a) and (b) Potentiodynamic polarization curves, (c) and (d) Nyquist plots and e) equivalent circuit of the as-cast and the heat-treated Mg-1.44Nd and Mg-1.43Ce alloys in a 0.9% NaCl solution.

Accordingly, the anodic branches in the polarisation curve represent the dissolution of Mg metal, while the cathodic branches represent the hydrogen evolution reaction and can be expressed by the following equations [31, 32]:
Anodic reaction:

$$Mg \rightarrow Mg^{2+} + 2e^{-} \quad (1)$$

Cathodic reaction:

$$H_2O + 2e^{-} \rightarrow 2OH^{-} + H_2 \quad (2)$$

Thus, the corrosion reaction of Mg-based alloys in aqueous solution leads to the formation of $Mg(OH)_2$ accompanied by hydrogen evolution:
The total reaction:

$$Mg + H_2O \rightarrow Mg(OH)_2 + H_2 \quad (3)$$

Both Mg-1.44Nd and Mg-1.43Ce alloys show similar trends. The hydrogen evolution rate (cathodic part of the polarisation curve) of the heat-treated alloys is lower than that of the as-cast alloys, indicating that heat treatment can decrease the hydrogen evolution on the cathodic process.

Table 2. Fitting parameters of the potentiodynamic polarization curves of the as-cast and the heat-treated Mg-1.44Nd and Mg-1.43Ce alloys in a 0.9% NaCl solution, respectively.

Mg-1.44Nd	**Ecorr (VSCE)**	**Icorr (μA.cm^{-2})**	**βa (VSCE)**	**βc (VSCE)**	**Rp (Ω cm^2)**
As-cast	-1.345	6.78	0.683	-0.112	5790
Heat-treated	-1.267	2.91	0.063	-0.179	6156
Mg-1.43Ce					
As-cast	-1.398	41.5	0.341	-0.127	970
Heat-treated	-1.039	0.86	0.099	-0.117	26890

Nevertheless, the anodic region varies depending on the conditions of the alloys.The as-castMg-1.44Nd and Mg-1.43Cealloys showed a similar passivation breakdown potential (E_b) at -0.75 V_{SCE}, indicating a tendency for localised corrosion such as pitting. The value of E_b for the present Mg-RE alloys is more positive compared tothe other Mg-based alloys[33], which means that these alloys are less susceptible to localised corrosion. Indeed, it was demonstrated that RE elements such as Dy, Gd, Nd, and Y have a weak ability for passivation in NaCl solution [34].

Table 2 shows that heat treatment shifts the E_{corr} for both alloys towards the noble direction (more positive) and decreases the I_{corr}-values, indicating an enhanced corrosion resistance. Interestingly, the present Mg-RE alloys were found to be nobler compared with several Mg-based alloys such as pure Mg [35], AZ31 [8] and Mg-2Zn (wt%) alloy[33] in 0.9% NaCl solution.

The polarisation resistance (R_p),which is inversely proportional to the corrosion rate, can be calculated using the Stern-Geary equation [36]:

$$R_p = \frac{\beta_a|\beta_c|}{2.303(\beta_a+|\beta_c|)I_{corr}} \quad (4)$$

The R_p values for the heat-treated alloys were much higher than those of the as-cast alloy, indicating that the heat-treated alloys were less susceptible to corrosion. The present results indicate that heat treatment improves the corrosion resistance of both alloys. Also, the heat-treated Mg-1.43Ce alloy (26890 Ω cm^2) seems to have very good corrosion resistance compared to the Mg-1.44Nd alloy (6156 Ω cm^2).

It has already been reported that binary high-pressure die-cast Mg-Ce alloy samples exhibited a lower corrosion rate than binary Mg-Nd and Mg-La alloys in 0.1 M NaCl (~0.6 wt% NaCl) solution [37]. In fact, the corrosion behaviour of Mg-RE alloys was found to be strongly affected by the specific *RE* element contained in the second phase [37]. Moreover, the results of the micro-capillary electrochemical cell method on $Mg_{12}Ce$, Mg_3Nd and $Mg_{12}La$ second phases show, firstly, that these second phases are significantly more stable than Mg and, secondly, that the $Mg_{12}Ce$ phase is the most inert compared to the other second phases [37].

Figures 3(c) and 3(d) present the Nyquist plots obtained from electrochemical impedance spectroscopy (EIS) for as-cast and heat-treated Mg-1.44Nd and Mg-1.43Ce alloys in a 0.9% NaCl solution, respectively. All samples show a small capacitive loop in the high-frequency region (~ 1780 Hz),resulting from the formation of a double layer and a charge transfer reaction between the metal interface and the solution [38]. The second capacitive loop is also shown in the medium-frequency region (in the range of 32-42 Hz), which may be attributed to the formation of corrosion product film and its resistance [38]. Finally, an inductive loop is formed in the low-frequency region (~ 0.04 Hz for Mg-1.44Nd and ~ 0.31 Hz for Mg-1.43Ce alloy), resulting from the occurrence of pitting corrosion and dissolution of the protective film [38].

In the present study, the similarity in Nyquist plots for all samples demonstrated that both alloys have similar corrosion mechanisms but with different rates, as shown by the difference in the diameters of the capacitive loops. As seen from Figure 3(d), the diameter of the capacitive loop in the medium-frequency region in the heat-treated Mg-1.43Ce alloy is considerably higher compared to the as-cast one, indicating good corrosion resistance of heat-treated Mg-1.43Ce alloy. In contrast, the diameters of capacitive loops and even the inductive loop are very similar in the case of as-cast and heat-treated Mg-1.44Nd alloy. Apparently, heating at 535 °C for 6 h slightly affects the corrosion mechanisms and rate of the Mg-1.44Nd alloy.

To further elucidate the corrosion mechanism of the studied alloys, the electrochemical equivalent circuit model proposed by Shi et al. [38] was adapted to fit the obtained Nyquist curves as presented in Figure 3(e); the corresponding fitting data are listed in Table 3, respectively.

Table 3. Electrochemical parameters obtained from the fits of the experimental EIS data of the as-cast and the heat-treated Mg-1.44Nd and Mg-1.43Ce alloys in a 0.9% NaCl solution.

Alloys	**R_s ($\Omega.cm^2$)**	**CPE_{dl} ($F.cm^{-2}$)**		**R_{ct} ($\Omega.cm^2$)**	**CPE_f ($F.cm^{-2}$)**		**R_f ($\Omega.cm^2$)**	**L ($H.cm^{-2}$)**	**R_L ($\Omega.cm^2$)**	**R_p ($\Omega.cm^2$)**
		Y	***n***		***Y***	***n***				
Mg-1.43Nd										
As-cast	38.26	3.8×10^{-5}	0.76	66.13	2.13×10^{-5}	0.93	36.16	2707	293.2	136.58
Heat-treated	37.23	4.7×10^{-5}	0.76	49.31	2.1×10^{-5}	0.96	84.14	2651	381	155.46
Mg-1.44Ce										
As-cast	33.7	4.1×10^{-5}	0.79	61.3	3.04×10^{-5}	0.97	54.15	98.85	132.8	133.47
Heat-treated	44.14	4.1×10^{-5}	0.73	167.7	1.58×10^{-5}	0.98	137.4	312.6	359.6	311.25

In this case, R_s is the solution resistance, and CPE_{dl} and R_{ct} are constant phase elements of the electric double layer and the charge transfer resistance, respectively. CPE_f and R_f are the constant phase elements of the corrosion product film and the film resistance. A constant phase element (CPE) is defined by Y and n values and is usually used instead of the capacitance in the case of the non-homogeneity of the sample surface. L and R_L are inductance and inductance resistance, representing the dissolution of partial protective film on the surface of the alloy.

As can be seen, the resistance of charge transfers R_{ct} of the Mg-1.44Nd alloy decreases from the as-cast to the heat treatment condition (66.1 vs. 49.3 Ω.cm^2). In contrast, it greatly increases in the case of the Mg-1.43Ce alloy (61.3 vs. 167.7 Ω.cm^2). It has been reported that the increase in the R_{ct} value indicates a decrease in the dissolution rate of Mg metal [24].

The R_f of heat-treated Mg-1.44Nd and Mg-1.43Ce alloys is higher than that of as-cast alloys, showing that the corrosion product film in the heated condition has a better ability to protect the Mg metal against corrosion. The as-heated Mg-1.43Ce alloy shows the highest value R_f = 312.6 Ω.cm^2.

The polarisation corrosion R_p can be mainly calculated from the equivalent circuits, as follows [13]:

$$R_p = R_s + R_{ct} + \frac{R_f R_L}{R_f + R_L} \quad (5)$$

Table 3 shows that R_p increases with heat treatment and that Mg-1.43Ce exhibits the highest value (311.25Ω.cm^2). These results are in good agreement with those from potentiodynamic polarisation curves. The XRD patterns of as-cast and heat-treated Mg-1.44Nd and Mg-1.43Ce alloys after immersion in 0.9% NaCl for 2 h are illustrated in Figure 4. XRD patterns reveal the presence of the $MgCl_2$ phase in the surface of both alloys. The amount of the $MgCl_2$ phase seems to be higher in heat-treated Mg-1.44Nd alloy, as indicated by the high intensity of the peak at 2θ = 29.2°. MgO and $Mg(OH)_2$ have also been evidenced as corrosion products in Mg-based alloys immersed in aqueous solution. In fact, the corrosion product film on the Mg surface was found to consist of a thin inner MgO layer covered with $Mg(OH)_2$[39].

The formation of MgO corresponds to the following equilibrium equation:

$$2\ Mg + O_2 \rightarrow 2\ MgO \quad (6)$$

In the presence of water, the MgO oxide gradually transforms to $Mg(OH)_2$, as in the following equation [40]:

$$MgO + H_2O \rightarrow Mg(OH)_2 \quad (7)$$

Furthermore, the corrosion products morphologies with low and high magnifications and the corresponding EDS results from marked points of as-cast and heat-treated Mg-1.44Nd and Mg-1.43Ce alloys after immersion in 0.9% NaCl for 2 h are shown in Figure 5 and Table 4, respectively. The corrosion products for all samples are mainly composed of $Mg(OH)_2$ and MgO, as demonstrated in Table 4.

It can be clearly seen that as-castMg-1.44Nd andheat-treatedMg-1.43Ce and Mg-1.44Ndalloys are covered by a thick and irregular film of corrosion products. Some cracks can be observed on the surface of heat-treated Mg-1.44Nd alloy, as shown by the arrow in Figure 5c.

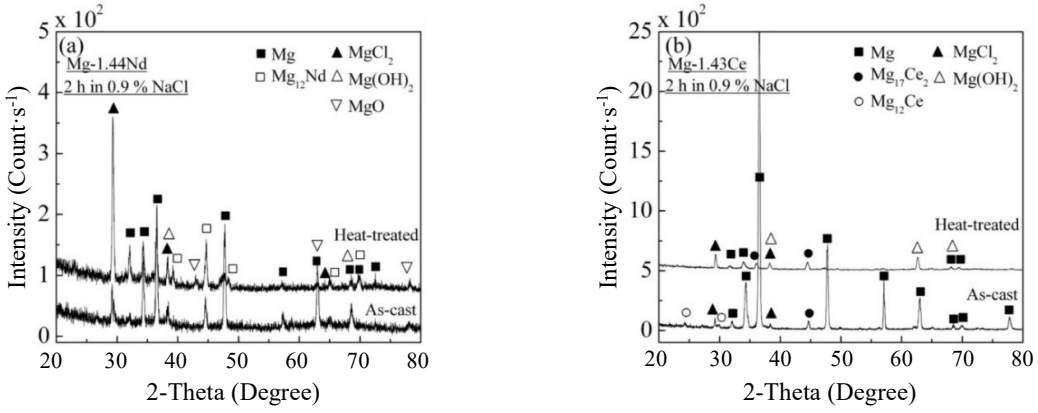

Figure 4. XRD patterns of the as-cast and the heat-treated: (a) Mg-1.44Nd and (b) Mg-1.43Ce alloys after immersion in 0.9% NaCl for 2 h.

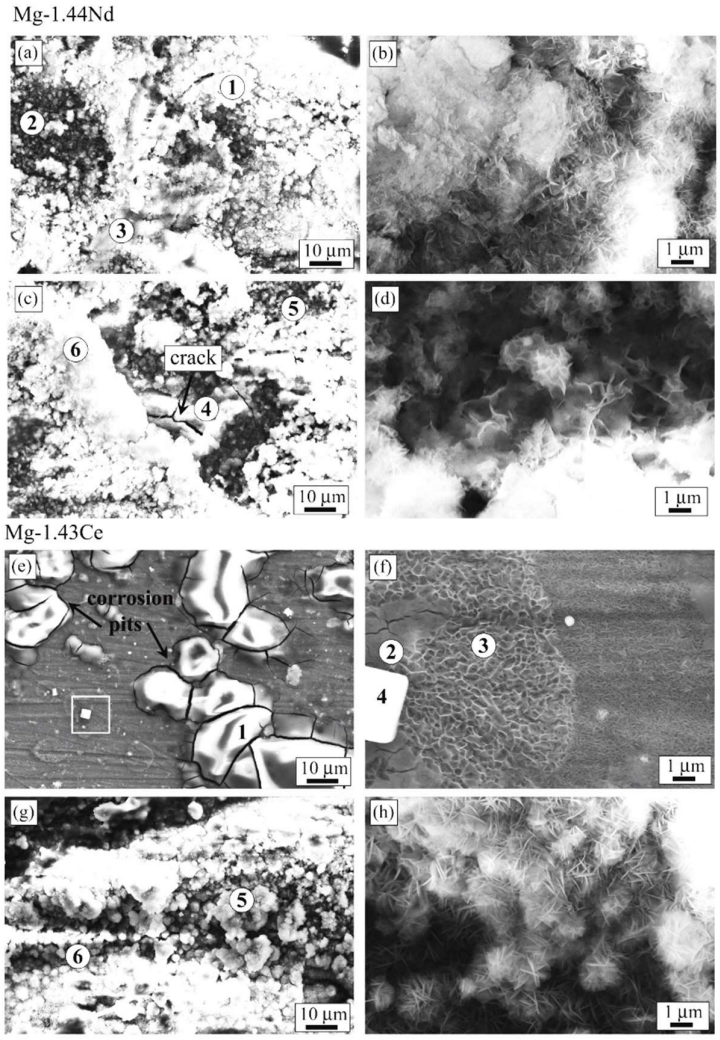

Figure 5. SEM micrographs showing corrosion products morphologies of (a) and (b) as-cast Mg-1.44Nd, (c) and (d) heat-treated Mg-1.44Nd, (e) and (f) as-cast Mg-1.43Ce and (g) and (h) heat-treated Mg-1.43Ce alloy after immersion in 0.9% NaCl for 2 h.

Table 4. EDS analysis at several positions in the surface (shown in Figure 5) of the as-cast and the heat-treated Mg-1.44Nd and Mg-1.43Ce alloys after immersion in 0.9% NaCl for 2 h, respectively.

Mg-1.44Nd						
Element (wt%)	**1**	**2**	**3**	**4**	**5**	**6**
C	1.14	-	-	2.47	-	-
O	2.74	39.48	51.38	45.79	38.25	58.08
Mg	41.87	60.2	48.18	40.93	61.42	41.88
Cl	6.02	-	-	10.53	-	-
Nd	0.23	0.32	0.43	0.29	0.33	0.04
Mg-1.43Ce						
Element (wt%)	**1**	**2**	**3**	**4**	**5**	**6**
C	0.64	2.99	-	-	-	-
O	52.36	41.88	40.49	17.98	38.55	33.02
Mg	42.67	41.71	58.58	47.95	58.95	66.33
Cl	4.02	11.42	-	-	-	-
Ce	0.3	1.99	0.93	34.07	2.5	0.65

A relatively high amount of Cl (10%) is present in these cracks (point 4). At high magnification, the surface of corroded Mg-1.44Nd and Mg-1.43Ce alloys shows needle-shaped aggregates, the length of which is much less in the Mg-1.43Ce alloy. Moreover, the EDS analysis of the corrosion products indicates that the $Mg(OH)_2$ film may contain some chloride Cl ions. It is worth noting that the Cl ions were absent in the corrosion product of heat-treated Mg-1.43Ce alloy. The presence of Cl ions accelerates the dissolution of the protective film and causes the corrosion rate to increase by transforming the $Mg(OH)_2$ into more soluble $MgCl_2$ [41,42]. In fact, it was demonstrated that the influence of chloride ion concentration on the corrosion product was larger in the solution containing low chloride concentrations [42,43].

The surface of the as-cast Mg-1.43Ce alloy exhibits totally different morphology (Figure 5(e)). The surface of the sample suffers from corrosion pits, and white coloured phase that is observed at the top of the cracks and which was identified as Mg(OH)2 (point 1). The formation of corrosion pits in the as-cast Mg-1.43Ce alloy could be attributed to the presence of second phases along the grains boundaries.

Recently it was demonstrated that the role of second phases containing RE element on the pitting corrosion of Mg-RE alloys was completely different from the role of second phases in non-RE Mg-based alloys[44-46]. It is well established that the occurrence of the pitting corrosion is caused by the second phases acting as micro-cathode in traditional Mg-based alloys such as AZ91 (Mg-9Al-1Zn, wt%) alloy [13]. Because RE elements are more active than Mg, it was demonstrated that the second phases in Mg-RE based alloys preferentially dissolved at the initial corrosion stage by acting as micro-anodes [44-46]. It was found that the pitting corrosion in Mg-RE alloys involved three stages. Firstly, the anodic phase dissolved followed by the corrosion of the Mg matrix and then the pitting corrosion appeared along with the depth of the dissolved phases [45].

The high magnification of the square zone shows an interesting feature (Figure 5(f)), in which the particles are surrounded by micro-cracks (point 2) and two distinct morphologies of needle-shaped clusters. The needle-like aggregates are longer and thinner (~400 nm) in the vicinity of the Ce particle and their morphology seems to change with increasing distance from the Ce particle. Far from the Ce particle (~ 7 μm), these aggregates decrease in size to ~100 nm and seem to be denser. The needle-shaped aggregates were identified as the corrosion product $Mg(OH)_2$ (point 3 in Figure 5(f) and Table 4). Such corrosion morphology has been largely reported in Mg-based alloys and it has been suggested that the film is more protective when the needles are smaller and denser [47].

Visibly, the corrosion product film contains an RE element, as shown in Table 4, and the concentration of the Ce element is relatively higher than the Nd element, which could explain the good corrosion resistance of Mg-1.43Ce alloy compared to Mg-1.44Nd alloy.

To summarise, based on the evolution of the microstructures of both alloys after heat treatment (Figure 1), the relative improvement in corrosion resistance of the Mg-1.44Nd alloy is attributed to the increase of the volume fraction of the second phase and their continuous distribution in the microstructure; that is, they act as a barrier against corrosion. By contrast, the great improvement in the corrosion resistance of the Mg-1.43Ce alloy is mainly due to the dissolution of the second phase in the vicinity of the grains boundaries, which prevents galvanic corrosion from occurring. The XRD results shown in Figure 2 suggest that the orientation of grains may also contribute to the improvement of the corrosion resistance of heat-treated alloys. Grains having (001) basal texture were found more corrosion resistant than (100) prismatic or other differently oriented ones in AZ31 alloy and pure Mg immersed in NaCl solution [18, 19]. The reduction of Mg dissolution in grain with basal (001) orientation was attributed to the closely packed crystallographic plane (001) with higher atomic coordination, tighter atomic bond and lower surface energy [19].

The present results help to understand more the relationship between the amount, the distribution of second phases and the corrosion response and thereby increasing the performance of Mg-based alloys as structural materials. An interesting finding was the fact that the corrosion resistance was found strongly depending on the specific RE alloying element. In the future, it will be interesting to focus on the effect of different RE alloying elements and their optimal concentrations on the corrosion behaviour of Mg-based alloys. Such knowledge helps to design new generation of Mg-based alloy with better controllable corrosion behaviour.

4. Conclusion

- The effect of heat treatment at 535°C for 6 h on the microstructure and corrosion behaviour of as-cast Mg-1.44Nd and Mg-1.43Ce alloys in a 0.9% NaCl solution was investigated.
- It was found that heat treatment leads to a more uniform distribution of the second phases in the Mg-1.44Nd alloy and their dissolution along the grains boundaries in the Mg-1.43Ce alloy.
- The uniform distribution of second phases in the microstructure may improve the corrosion resistance, as shown in Mg-1.44Nd alloy. Indeed, the dissolution of the second phases along the grain boundaries significantly improves the corrosion resistance, as evidenced in the case of Mg-1.43Ce alloy.
- For both alloys, the corrosion products comprise magnesium hydroxide $Mg(OH)_2$ and magnesium oxide MgO.

- Corrosion morphologies depend strongly on the distribution of the second phase. The as-cast Mg-1.43Ce alloy suffers from pitting corrosion, owing to the presence of the second phase in the grain boundaries. More uniform corrosion was found in heat-treated alloys, owing to the homogeneous distribution of the second phases.

5. Acknowledgements

The authors gratefully acknowledge Dr. Talal Al-Samman; Institute für Metallkunde und Metallphysik (IMM-RWTH), Aachen, Germany, for supplying the Mg-RE alloys. This work was supported by the PRFU national project under Grant Agreement No. B00L02UN280120180005.

References

[1] J. Hirsch and T. Al-Samman, "Superior light metals by texture engineering: Optimized aluminum and magnesium alloys for automotive applications," *Acta Materialia*, vol. 61, pp. 818-843, 2013.

[2] S. You, Y. Huang, K. U. Kainer, and N. Hort, "Recent research and developments on wrought magnesium alloys," *Journal of Magnesium and Alloys*, vol. 5, pp. 239-253, 2017.

[3] A. Atrens, S. Johnston, Z. Shi, and M. S. Dargusch, "Viewpoint-Understanding Mg corrosion in the body for biodegradable medical implants," *Scripta Materialia*, vol. 154, pp. 92-100, 2018.

[4] A. Atrens, G.-L. Song, M. Liu, Z. Shi, F. Cao, and M. S. Dargusch, "Review of Recent Developments in the Field of Magnesium Corrosion," *Advanced Engineering Materials*, vol. 17, pp. 400-453, 2015.

[5] T. B. Abbott, "Magnesium: Industrial and Research Developments Over the Last 15 Years," *Corrosion*, vol. 71, pp. 120-127, 2015.

[6] Y. Unigovski, L. Riber, and E. Gutman, "Corrosion Stress Relaxation in Pure Magnesium and Die-Cast Mg Alloys," *Journal of Metals, Materials and Minerals*, vol. 17, pp. 1-7, 2007.

[7] R. L. Liu, J. R. Scully, G. Williams, and N. Birbilis, "Reducing the corrosion rate of magnesium via microalloying additions of group 14 and 15 elements," *Electrochimica Acta*, vol. 260, pp. 184-195, 2018.

[8] N. Saikrishna, G. P. K. Reddy, B. Munirathinam, and B. R. Sunil, "Influence of bimodal grain size distribution on the corrosion behavior of friction stir processed biodegradable AZ31 magnesium alloy," *Journal of Magnesium and Alloys*, vol. 4, pp. 68-76, 2016.

[9] C. L. P. Silva, A. C. X. Oliveira, C. G. F. Costa, R. B. Figueiredo, M. de Fátima Leite, M. de Magalhães Pereira, V. F. C. Lins, and T. G. Langdon, "Effect of severe plastic deformation on the biocompatibility and corrosion rate of pure magnesium," *Journal of Materials Science*, vol. 52, pp. 5992-6003, 2017.

[10] H. Feng, S. Liu, Y. Du, T. Lei, R. Zeng, and T. Yuan, "Effect of the second phases on corrosion behavior of the Mg-Al-Zn alloys," *Journal of Alloys and Compounds*, vol. 695, pp. 2330-2338, 2017.

[11] J. Li, Q. Jiang, H. Sun, and Y. Li, "Effect of heat treatment on corrosion behavior of AZ63 magnesium alloy in 3.5wt% sodium chloride solution," *Corrosion Science*, vol. 111, pp. 288-301, 2016.

[12] A. Hanna, A. Dakhouche, K. Tirsatine, A. Sari, Y. Khereddine, D. Bradai, and H. Azzeddine, "Effect of hot rolling on the corrosion behavior of AZ31 magnesium alloy," *Metallurgical Research & Technology*, vol. 116, p. 109, 2019.

[13] T. Zhang, Y. Shao, G. Meng, Z. Cui, and F. Wang, "Corrosion of hot extrusion AZ91 magnesium alloy: I-relation between the microstructure and corrosion behavior," *Corrosion Science*, vol. 53, pp. 1960-1968, 2011.

[14] T. Zhang, G. Meng, Y. Shao, Z. Cui, and F. Wang, "Corrosion of hot extrusion AZ91 magnesium alloy. Part II: Effect of rare earth element neodymium (Nd) on the corrosion behavior of extruded alloy," *Corrosion Science,* vol. 53, pp. 2934-2942, 2011.

[15] G. M. Naik, N. S, and S. Kumar, "Corrosion of ECAPed magnesium alloys and its background: A Review," *Journal of Metals, Materials and Minerals*, vol. 29, pp. 1-20, 2019.

[16] D. Song, A. Ma, J. Jiang, P. Lin, D. Yang, and J. Fan, "Corrosion behavior of equal-channel-angular-pressed pure magnesium in NaCl aqueous solution," *Corrosion Science*, vol. 52, pp. 481-490, 2010.

[17] D. Song, A. B. Ma, J. H. Jiang, P. H. Lin, D. H. Yang, and J. F. Fan, "Corrosion behaviour of bulk ultra-fine grained AZ91D magnesium alloy fabricated by equal-channel angular pressing," *Corrosion Science*, vol. 53, pp. 362-373, 2011.

[18] R. Xin, B. Li, L. Li, and Q. Liu, "Influence of texture on corrosion rate of AZ31 Mg alloy in 3.5wt% NaCl," *Materials & Design*, vol. 32, pp. 4548-4552, 2011.

[19] G.-L. Song and Z. Xu, "Crystal orientation and electrochemical corrosion of polycrystalline Mg," *Corrosion Science*, vol. 63, pp. 100-112, 2012.

[20] J. He, B. Jiang, J. Xu, J. Zhang, X. Yu, B. Liu, and F. Pan, "Effect of texture symmetry on mechanical performance and corrosion resistance of magnesium alloy sheet," *Journal of Alloys and Compounds*, vol. 723, pp. 213-224, 2017.

[21] T. Takenaka, T. Ono, Y. Narazaki, Y. Naka, and M. Kawakami, "Improvement of corrosion resistance of magnesium metal by rare earth

elements," *Electrochimica Acta*, vol. 53, pp. 117-121, 2007.

[22] J. Meng, W. Sun, Z. Tian, X. Qiu, and D. Zhang, "2-Corrosion performance of magnesium (Mg) alloys containing rare-earth (RE) elements," in *Corrosion Prevention of Magnesium Alloys*, G.-L. Song, Ed., ed: Woodhead Publishing, 2013, pp. 38-60.

[23] F. Rosalbino, E. Angelini, S. De Negri, A. Saccone, and S. Delfino, "Electrochemical behaviour assessment of novel Mg-rich Mg–Al–RE alloys (RE=Ce, Er)," *Intermetallics*, vol. 14, pp. 1487-1492, 2006.

[24] S. D. Wang, D. K. Xu, X. B. Chen, E. H. Han, and C. Dong, "Effect of heat treatment on the corrosion resistance and mechanical properties of an as-forged Mg–Zn–Y–Zr alloy," *Corrosion Science*, vol. 92, pp. 228-236, 2015.

[25] X.-b. Liu, D.-y. Shan, Y.-w. Song, and E.-h. Han, "Effects of heat treatment on corrosion behaviors of Mg-3Zn magnesium alloy," *Transactions of Nonferrous Metals Society of China*, vol. 20, pp. 1345-1350, 2010.

[26] G. Song, A. L. Bowles, and D. H. StJohn, "Corrosion resistance of aged die cast magnesium alloy AZ91D," *Materials Science and Engineering: A*, vol. 366, pp. 74-86, 2004.

[27] G. Song, A. Atrens, and M. Dargusch, "Influence of microstructure on the corrosion of diecast AZ91D," *Corrosion Science*, vol. 41, pp. 249-273, 1998.

[28] S. Manivannan, S. K. Gopalakrishnan, S. P. Kumaresh Babu, and S. Sundarrajan, "Effect of cerium addition on corrosion behaviour of AZ61+XCe alloy under salt spray test," *Alexandria Engineering Journal*, vol. 55, pp. 663-671, 2016.

[29] Y. I. Bourezg, H. Azzeddine, T. Baudin, A.-L. Helbert, Y. Huang, D. Bradai, and T. G. Langdon, "Texture and microhardness of Mg-Rare Earth (Nd and Ce) alloys processed by high-pressure torsion," *Materials Science and Engineering: A*, vol. 724, pp. 477-485, 2018.

[30] L. L. Rokhlin, Magnesium Alloys Containing Rare Earth Metals: Structure and Properties: Taylor & Francis, 2003.

[31] J.-W. Chang, X.-W. Guo, P.-H. Fu, L.-M. Peng, and W.-J. Ding, "Effect of heat treatment on corrosion and electrochemical behaviour of Mg–3Nd–0.2Zn–0.4Zr (wt%) alloy," *Electrochimica Acta*, vol. 52, pp. 3160-3167, 2007.

[32] G. L. Song and A. Atrens, "Corrosion mechanisms of magnesium alloys," *Advanced Engineering Materials*, vol. 1, pp. 11-33, 1999.

[33] H. Jia, X. Feng, and Y. Yang, "Microstructure and corrosion resistance of directionally solidified Mg-2wt% Zn alloy," *Corrosion Science*, vol. 120, pp. 75-81, 2017.

[34] X. Zhao, L.-l. Shi, and J. Xu, "A comparison of corrosion behavior in saline environment: rare earth metals (Y, Nd, Gd, Dy) for alloying of biodegradable magnesium alloys," *Journal of Materials Science & Technology*, vol. 29, pp. 781-787, 2013.

[35] J. Fernández, Y. El Ouardi, J. Bonastre, J. M. Molina, and F. Cases, "Modification of the magnesium corrosion rate in physiological saline 0.9 wt% NaCl via chemical and electrochemical coating of reduced graphene oxide," *Corrosion Science*, vol. 152, pp. 75-81, 2019.

[36] D.-J. Lin, F.-Y. Hung, M.-L. Yeh, H.-P. Lee, and T.-S. Lui, "Development of a novel micro-textured surface using duplex surface modification for biomedical Mg alloy applications," *Materials Letters*, vol. 206, pp. 9-12, 2017.

[37] N. Birbilis, M. A. Easton, A. D. Sudholz, S. M. Zhu, and M. A. Gibson, "On the corrosion of binary magnesium-rare earth alloys," *Corrosion Science*, vol. 51, pp. 683-689, 2009.

[38] Z. Shi, F. Cao, G.-L. Song, M. Liu, and A. Atrens, "Corrosion behaviour in salt spray and in 3.5% NaCl solution saturated with Mg(OH)2 of as-cast and solution heat-treated binary Mg–RE alloys: RE=Ce, La, Nd, Y, Gd," *Corrosion Science*, vol. 76, pp. 98-118, 2013.

[39] M. Santamaria, F. Di Quarto, S. Zanna, and P. Marcus, "Initial surface film on magnesium metal: A characterization by X-ray photoelectron spectroscopy (XPS) and photocurrent spectroscopy (PCS)," *Electrochimica Acta*, vol. 53, pp. 1314-1324, 2007.

[40] H. B. Yao, Y. Li, and A. T. S. Wee, "An XPS investigation of the oxidation/corrosion of melt-spun Mg," Applied Surface Science, vol. 158, pp. 112-119, 2000.

[41] R. Ambat, N. N. Aung, and W. Zhou, "Evaluation of microstructural effects on corrosion behaviour of AZ91D magnesium alloy," *Corrosion Science*, vol. 42, pp. 1433-1455, 2000.

[42] H. Altun and S. Sen, "Studies on the influence of chloride ion concentration and pH on the corrosion and electrochemical behaviour of AZ63 magnesium alloy," *Materials & Design,* vol. 25, pp. 637-643, 2004.

[43] M.-C. Zhao, M. Liu, G.-L. Song, and A. Atrens, "Influence of pH and chloride ion concentration on the corrosion of Mg alloy ZE41," *Corrosion Science*, vol. 50, pp. 3168-3178, 2008.

[44] J. Liu, Y. Song, J. Chen, P. Chen, D. Shan, and E.-H. Han, "The Special Role of Anodic Second Phases in the Micro-galvanic Corrosion of EW75 Mg Alloy," *Electrochimica Acta*, vol. 189, pp. 190-195, 2016.

[45] Y. Song, D. Shan, and E.-H. Han, "Pitting corrosion of a Rare Earth Mg alloy GW93," *Journal of Materials Science & Technology*, vol. 33, pp. 954-960, 2017.

[46] C. Cai, R. Song, L. Wang, and J. Li, "Effect of anodic T phase on surface micro-galvanic corrosion of biodegradable Mg-Zn-Zr-Nd alloys," *Applied Surface Science*, vol. 462, pp. 243-254, 2018.

[47] Y. Song, E.-H. Han, K. Dong, D. Shan, C. D. Yim, and B. S. You, "Study of the corrosion product films formed on the surface of Mg–xZn alloys in NaCl solution," *Corrosion Science*, vol. 88, pp. 215-225, 2014.